Hindawi
Journal of Electrical and Computer Engineering
Volume 2022, Article ID 7645777, 16 pages
https://doi.org/10.1155/2022/7645777

Research Article

Robust Power Designing of Supplementary Damping Controller in VSC HVDC System to Improve Energy Conversion Efficiency of Wind Turbine and Power System Stability

A. Hamidi, J. Beiza, T. Abedinzadeh, and A. Daghigh

Department of Electrical Engineering, Shabestar Branch, Islamic Azad University, Shabestar, Iran

Correspondence should be addressed to J. Beiza; j.beiza@iaushab.ac.ir

Received 8 October 2021; Revised 30 November 2021; Accepted 6 December 2021; Published 12 January 2022

Academic Editor: François Vallée

Because of low losses and voltage drop, fast control of power, limitless connection distance, and isolation issues, using high-voltage direct-current (HVDC) transmission system is recommended to transfer power in the power systems, including wind farms. This paper aims to propose a supplementary damping controller (SDC) based on the HVDC to improve not only power system dynamic stability but also energy conversion efficiency and torsional vibration damping in the wind power plants (WPPs). When the WPPs are working in power control mode, the active power is set to its reference value, which is extracted from power-speed curve. This paper shows that torsional oscillations associated with the poorly torsional modes can be affected by different operating regions of the power-speed curve of WPP. Therefore, it is essential to employ an SDC to have the optimum energy conversion efficiency in the wind turbine and the most dynamic stability margin in the power system. The SDC is designed using a fractional-order PID controller (FOPID) based on the multiobjective bat-genetic algorithm (MOBGA). The simulation results show that the proposed control strategy effectively works in minimizing the torsional and electromechanical oscillations in power system and optimizing the energy conversion efficiency in the wind turbine.

1. Introduction

Nowadays, due to the increased energy demand and environmental considerations, there is a growing need for using renewable energy sources, such as wind energy, in power systems [1–5]. Having different structure and performance compared to the classic power plants, the rapid growth of WPPs in the power systems has raised concerns for transmission system operators [4–7]. The oscillating nature of wind energy can affect the efficiency of energy conversion in the wind turbine as well as the exchanged power between the wind farm and main grid [8–10]. Also, most wind WPPs use the induction generators in their structure and therefore can effect on reactive power flow and voltage profile at the point of common coupling (PCC). From an electromechanical perspective, the flexible drive chain of the wind turbine generates long-term torsional oscillation, which causes significant stresses and fatigue loss of gearbox [11–14]. The oscillations of the mechanical components can be transmitted to electrical power and frequency, leading to potential resonances between wind turbine and the power system [15–18]. Therefore, the power system operators need to utilize new requirements and standards for the integration of wind farms and common power systems.

To improve the performance of power systems that include WPPs, the use of supplementary controllers and compensators along with the FACTS devices and HVDC transmission systems has been suggested [19–21]. The most important advantages of these technologies are as follows: (a) control the active and reactive power exchange flexibly and independently, (b) improve the power quality, (c) enhance the system transient and dynamic stability, and (d) damp interarea oscillation modes [22–25].

The voltage source converter- (VSC-) based HVDC systems have advanced controllability and are capable of providing grid support to the connected AC networks

[10–13]. This technology has the advantage of fast response, the possibility of providing reactive power to AC systems, and the use of supplementary control signals to their automatic voltage regulators to improve dynamic and transient (voltage-frequency) stability, damp local and interarea oscillations, and mitigate subsynchronous shaft torsional oscillation in power systems, including WPPs [22–25].

In [26], a method based on hybrid particle Swarm Optimization in order to design a WADC that ensures robustness to power system operating uncertainties, time delays variations on the WADC channels, and the permanent failure of the WADC communication channels is proposed. Although the proposed WADC has improved the dynamic stability of the power system, the effect of the wind turbine characteristic curve on the damping of the oscillation modes of the network has not been studied. In [27], a new, robust control design of power oscillation damper (POD) for a DFIG-based wind turbine using a specified structure mixed H2/HN control is proposed. The proposed robust POD increases the dynamic complexity of the power system. In addition, the ability of the proposed controller to operate in different operating conditions of the wind turbine in DFIG has not been investigated. In [28], a power system stabilizer (PSS) for a wind turbine employing a doubly fed induction generator (DFIG) is proposed. It is shown that the proposed controller has improved the dynamic stability margin of the power system appropriately. However, the interaction of the oscillation modes of the wind turbine and synchronous generators has not been evaluated based on the presented dynamic model of power system. In addition, the variable working conditions of wind turbine have not been taken into account. In [29], to enhance the robustness of stabilizing controllers against system uncertainties, a new coordinated robust control of doubly fed induction generator (DFIG) wind turbine equipped with power oscillation damper (POD) and synchronous generator installed with power system stabilizer (PSS) for stabilization of power system oscillations is proposed. However, the effect of the control signal on the oscillation modes of the power system has not been evaluated based on the wind turbine power-speed characteristic curve.

As mentioned above, in many proposed methods for the designing damping controllers in WPP, the effects of the wind turbine characteristic curve on the damping coefficient of oscillation modes have not been considered. However, in this paper, it is shown that depending on the operating conditions of the WPP, the damping torque injected into the system is different and to amplify this torque, a supplementary damping controller in the active power control loop of WPP is proposed. It is also shown that the control inputs of the HVDC system are effective on the oscillation modes of the power system equipped with WPP, and therefore to strengthen the dynamic stability margin, the use of a damping controller in the HVDC transmission system is suggested. The proposed damping controllers in WPP and HVDC can suppress the torsional vibrations and enhance the energy conversion efficiency in the drive train system of WPP. In the present work, using a FOPID based on EMA is utilized to design SDC controller.

2. The Modeling of Hybrid Power System

Figure 1 shows the power system under study which includes the WPP, the classical power plant, and the VSC HVDC transmission system. It can be assumed that WPP is connected to the network through an electronic-power convert. V', V_r, V_i, V_b' are points of common coupling, rectifier, inverter, and infinite bus voltage, respectively. X_t, X_l are reactance of coupling transformers. $I_w, I, I_{\text{Temp}}, I_r, I_i, I_L$ are currents of wind farm, classic power plant, AC transmission line, rectifier, inverter, and load, respectively. $M_r, \theta_r\,(PH_r)$ and $M_i, \theta_i\,(PH_i)$ are phase angle and modulation index for rectifier and inverter, respectively. The wind farm consists of the constant wind speed turbines equipped by the squirrel cage induction generators. For a dynamic study, an integrated model for the whole wind farm can be used; state variables are $\omega_t, s, \theta_g, E_{wd}', E_{wq}', V_{dcr}, I_d, V_{dci}, \omega, \delta, E_q', E_{fd}$.

And the input signals are $M_r, \theta_r, M_i, \theta_i, U_{pss}, T_w$.

The mentioned variables are used to model the power system under study. In this paper, the dynamic model of power system that is proposed in [1, 17] is used.

The performance of the DC transmission line can be described by using the following equations:

$$\begin{aligned}
\Delta \dot{V}_{dci} &= \frac{1}{C}\left\{C_{75}\Delta\delta + C_{74}\Delta V_{dci} + C_{73}\Delta m_i + C_{72}\Delta\theta_i + \Delta I_d\right\},\\
\Delta \dot{I}_d &= \frac{1}{L}\left\{\Delta V_{dcr} - R\Delta I_d - \Delta V_{dci}\right\},\\
\Delta \dot{V}_{dcr} &= \frac{1}{C}\left\{C_{56}\Delta\delta + C_{53}\Delta E_q' + C_{59}\Delta E_{wd}' + C_{58}\Delta E_{wq}' + C_{57}\Delta V_{dcr} + C_{54}\Delta m_r - \Delta I_d + C_{55}\Delta\theta_r\right\}.
\end{aligned} \tag{1}$$

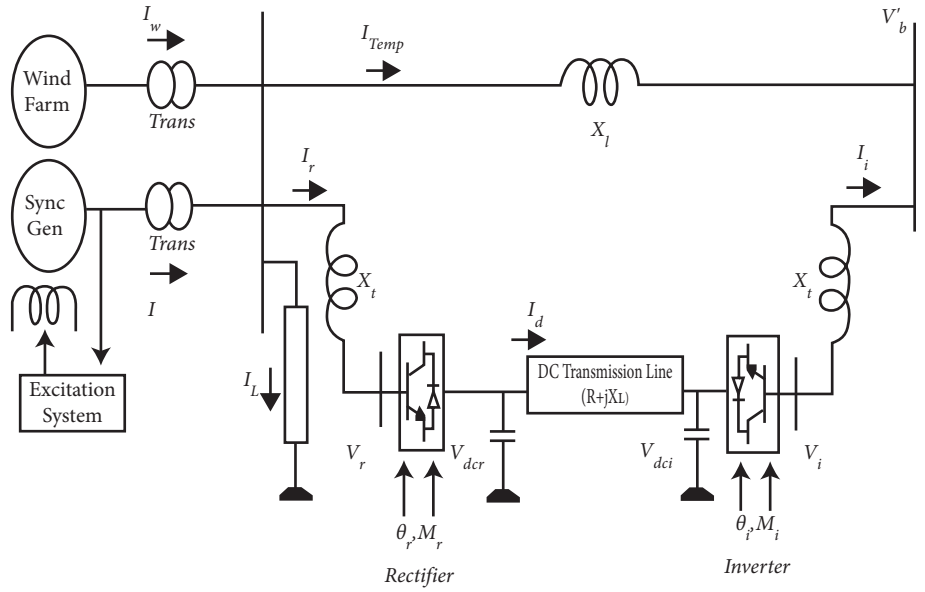

Figure 1: The power system under study.

Also, the linearized dynamic model of the synchronous generator can be shown by the following equations:

$$\begin{aligned}
\Delta\dot{\delta} &= \omega_b \Delta\omega,\\
\Delta\dot{\omega} &= \frac{1}{M}\left\{-C_{81}\Delta\delta - C_{78}\Delta E'_q - D\Delta\omega - C_{82}\Delta E'_{wd} - C_{83}\Delta E'_{wq} - C_{79}\Delta m_r - C_{80}\Delta\theta_r\right\},\\
\Delta\dot{E}'_q &= \frac{1}{T'_{do}}\left\{\Delta E_{fd} - \left(X_d - X'_d\right)\left(C_{19}\Delta E'_q + C_{20}\Delta m_r + C_{21}\Delta\theta_r + C_{22}\Delta\delta + C_{23}\Delta E'_{wq} + C_{24}\Delta E'_{wd}\right) - \Delta E'_q\right\},\\
\Delta\dot{E}_{fd} &= \frac{1}{T_A}\left\{-K_A C_{90}\Delta\delta - K_A C_{87}\Delta E'_q - \Delta E_{fd} - K_A C_{19}\Delta E'_{wd} - K_A C_{92}\Delta E'_{wq} + K_A\Delta U_{PSS} - K_A C_{88}\Delta m_r - K_A C_{89}\Delta\theta_r\right\}.
\end{aligned} \tag{2}$$

For the wind farm, the mechanical equations for the drive train are considered. The drive train is shown in Figure 2. In this model, θ_{tg} is the angular displacement of the rotor in WPP; ω_t ω_g, H_t, and H_g are the turbine, generator angular speed, and the corresponding inertia constants, respectively. K, D are the damping constants. T_t and T_e point to the wind and electromagnetic torques.

Using Figure 2, we can write ($\omega_g = (1 - S)\omega_{\text{synchronous}}$):

$$\begin{aligned}
2H_t\frac{d\omega_t}{dt} &= T_t - K\theta_{tg} - D\left(\omega_t - \omega_g\right),\\
\Delta\dot{\omega}_t &= \frac{1}{2H_t}\left\{\Delta T_t - K\Delta\theta_{tg} + D\Delta\omega_t - D\Delta\omega_g\right\},\\
2H_g\frac{d\omega_g}{dt} &= K\theta_{tg} + D\left(\omega_t - \omega_g\right) - T_{e-\text{wind}},\\
\Delta\dot{\omega}_g &= \frac{1}{2H_g}\left\{-\Delta T_{e-\text{wind}} + K\Delta\theta_{tg} + D\left(\Delta\omega_t - \Delta\omega_g\right)\right\}.
\end{aligned} \tag{3}$$

Transient states and saturation of the damper and stator windings are neglected. Considering E'_w as the induced voltage in machine and I_w as the injected current to PCC, it is possible to write the following equations for the electrical torque (in per unit):

$$\begin{aligned}
T_{e-\text{wind}} &= P_{e-\text{wind}},\\
T_{e-\text{wind}} &= E'_{wd}I_{wd} + E'_{wq}I_{wq},\\
\Delta T_{e-\text{wind}} &= \Delta E'_{wd}I_{wd} + E'_{wd}\Delta I_{wd} + \Delta E'_{wq}I_{wq} + E'_{wq}\Delta I_{wq}.
\end{aligned} \tag{4}$$

The injected current components should be linearized for ΔT_e calculation. Using the proposed dynamic model in [1, 17], the following equation can be written:

$$\begin{aligned}
\Delta T_{e-\text{wind}} = {} & C_{90}\Delta E'_q + C_{91}\Delta m_r + C_{93}\Delta\theta_r + C_{92}\Delta\delta\\
& + C_{88}\Delta E'_{wd} + C_{89}\Delta E'_{wq}.
\end{aligned} \tag{5}$$

For the other states of the wind turbine, we can write

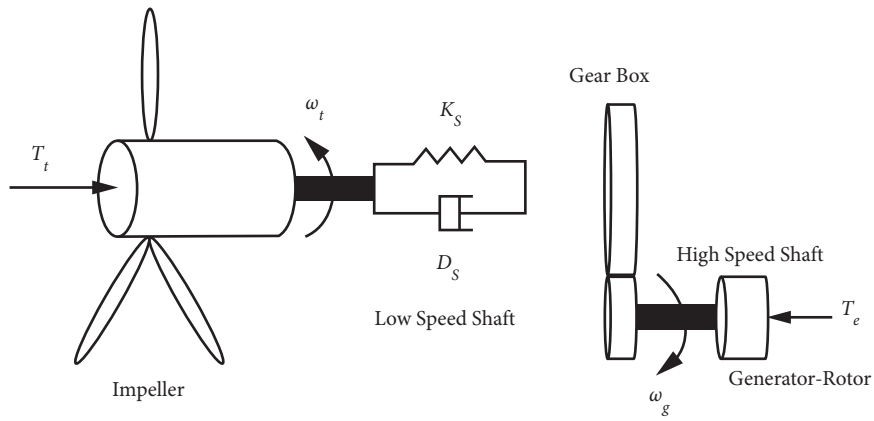

Figure 2: Drive train model.

$$\frac{d\theta_{tg}}{dt} = \omega_t - \omega_g,$$
$$\Delta\dot{\theta}_{tg} = \Delta\omega_t - \Delta\omega_g. \tag{6}$$

The internal voltage of the wind turbine can be shown as follows:

$$\frac{dE'_{wd}}{dt} = \frac{1}{T'_o}\left\{E'_{wd} - (X_w - X'_w)I_{wq}\right\} + S\omega_s E'_{wq},$$
$$\frac{dE'_{wq}}{dt} = \frac{1}{T'_o}\left\{E'_{wq} + (X_w - X'_w)I_{wd}\right\} - S\omega_s E'_{wd}. \tag{7}$$

Using the linearized model of equations (32) and (35) from [1], the induction machine external voltage can be written as follows:

$$\begin{aligned}\Delta\dot{E}'_{wd} &= C_{94}\Delta E'_{wd} + C_{95}\Delta E'_q + C_{96}\Delta m_r + C_{97}\Delta\theta_r \\ &\quad + C_{98}\Delta\delta + C_{99}\Delta S + C_{100}\Delta E'_{wq},\\ \Delta\dot{E}'_{wq} &= C_{106}\Delta E'_{wd} + C_{102}\Delta E'_q + C_{103}\Delta m_r + C_{104}\Delta\theta_r \\ &\quad + C_{105}\Delta\delta + C_{107}\Delta S + C_{101}\Delta E'_{wq}.\end{aligned} \tag{8}$$

The state space model of the power system can be shown by equations (1)–(8).

3. The Analysis of the Torsional Modes Performance in WPP

Before designing the SDC, it seems logical to identify the factors affecting the control of the tensional modes of the system. Identification of the influence of different factors can play a significant role in the proper design of the SDC. In this section of the paper, the factors affecting the torsional modes are studied.

Using the two-mass block model of the drive chain described in relations (30) and (34) from [1], the motion equation of the turbine relative to the angular displacement of the turbine-rotor shaft can be obtained as follows:

$$\begin{aligned}&\Delta\ddot{\theta}_{tg} + D\left(\frac{1}{2H_t} + \frac{1}{2H_g}\right)\Delta\dot{\theta}_{tg} \\ &\quad + K\left(\frac{1}{2H_t} + \frac{1}{2H_g}\right)\Delta\theta_{tg} = \frac{\Delta T_t}{2H_t} + \frac{\Delta T_{e-\text{wind}}}{2H_g}.\end{aligned} \tag{9}$$

As mentioned earlier, the mechanical torque (power) of the wind turbine varies depending on the wind speed. The following equations can be used to calculate from the wind turbine:

$$P_{t-\text{wind}} = P_{\text{wind}}C_p(\lambda,\beta),$$
$$P_{\text{wind}} = \frac{1}{2}\rho\pi R^2 V_w^3, \tag{10}$$

where P_{wind} is the extracted power from the wind, V_w is the wind speed, ρ is a function of tip-speed ratio, and is blade pitch angle. On the other hand, for the linearized torque-power relation, we can write

$$T_t = \frac{P_{t-\text{wind}}}{\omega_t},$$
$$\Delta T_t = \frac{-1}{\omega_{t0}^2}P_{t0}\Delta\omega_t + P_{\text{wind0}}\frac{\partial C_p(\lambda,\beta)}{\partial\lambda}\frac{d\lambda}{d\omega_t}\Delta\omega_t. \tag{11}$$

Regarding equation (40), it is observed that ΔT is influenced by V_w, C_p, and λ. It should be noticed that mechanical torque deviation of the wind turbine is affected by uncertainties of the wind speed and the pitch angle control.

In the power control mode of WPPs, the active power reference ($P_{s-\text{ref}}$) is calculated using the speed-power curve (Figure 3) as follows:

$$T_{e-\text{wind}} \cong P_{e-\text{wind-ref}} = f(\omega_g),$$
$$\Delta T_{e-\text{wind}} \cong \Delta P_{e-\text{wind-ref}} = f'(\omega_{g0})\Delta\omega_g, \quad \left(f' \equiv \frac{df}{d\omega_g}\right). \tag{12}$$

Based on equation (41), the electrical torque can be effective in mechanical torsional vibrations; however, this component depends on the reference value of the wind

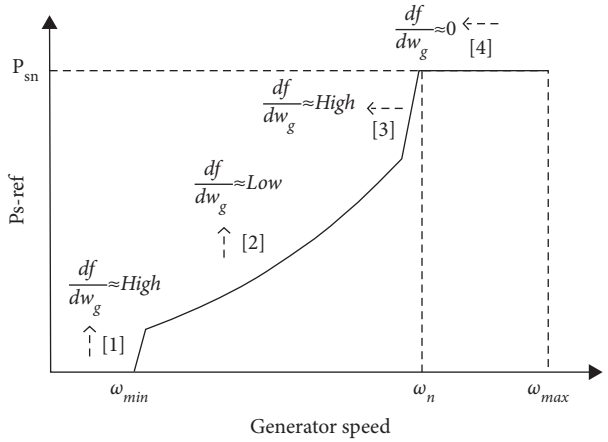

Figure 3: Speed-power curve of WPP.

power, which is determined by the speed-power curve of wind turbine. ΔT_e can produce a component of electrical torque proportional to the generator speed. As shown in Figure 3, the damping value provided by the electrical torque is dependent on $(\mathrm{d}f/\mathrm{d}\omega_g)$, which varies in the different working points. It is found that, unlike region (2), in regions (1) and (3) the appropriate damping is provided by the electrical torque for the tensional modes, whereas in region (4) the contribution of the electrical torque for damping tensional modes is zero. It is proposed to design a supplementary damping controller for WPP to obtain enough damping of torsional modes for regions (2) and (4).

Equations (40) and (41) show the effects of electrical and mechanical torques of the wind turbine on torsional modes. However, using equation (33) in relation (37), we can write

$$\Delta\ddot{\theta}_{tg} + D\left(\frac{1}{2H_t}+\frac{1}{2H_g}\right)\Delta\dot{\theta}_{tg} + K\left(\frac{1}{2H_t}+\frac{1}{2H_g}\right)\Delta\theta_{tg} = \frac{\Delta T_t}{2H_t} + \frac{1}{2H_g}\left(C_{90}\Delta E'_q + C_{91}\Delta m_r + C_{93}\Delta\theta_r + C_{92}\Delta\delta + C_{88}\Delta E'_{wd} + C_{89}\Delta E'_{wq}\right). \quad (13)$$

Transfer function with $\Delta m_r, \Delta\theta_r$, $\Delta T_{e-\mathrm{wind}}$, and ΔT_t as input variables can be further derived as shown in the following formulae:

$$\frac{\Delta\theta_{tg}}{\Delta T_{e-\mathrm{wind}}} = \frac{\left(1/2H_g\right)}{S^2 + A's + B'}, \quad (14)$$

$$\frac{\Delta\theta_{tg}}{\Delta T_t} = \frac{\left(1/2H_t\right)}{S^2 + A's + B'}. \quad (15)$$

The frequency domain characteristics of equations (14) and (15) are shown in Figure 4.

The following points can be concluded:

(i) The electrical and mechanical torques of the wind turbine influence the torsional vibrations (equations (11)–(13)).

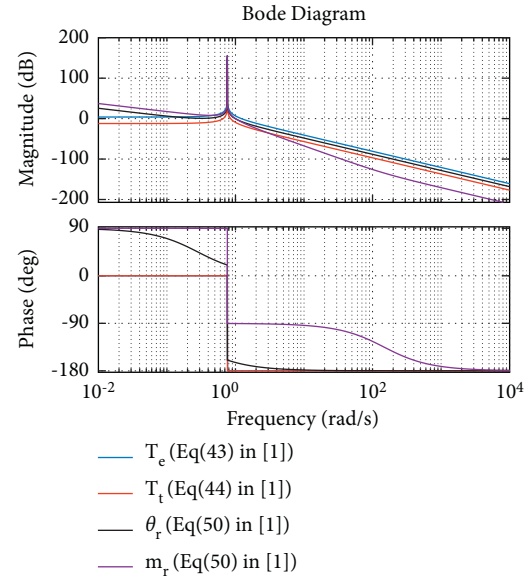

Figure 4: Bode characteristics of the input variables.

(ii) The amplitude gain of the drive chain near the resonance frequency in Figure 4 is very high; that is, any deviation of $\Delta m_r, \Delta\theta_r, \Delta T_t, \Delta T_e$ can excite the drive chain torsional modes.

(iii) The magnitude of $\Delta T_{e-\mathrm{wind}}$ at the resonance frequency is larger than ΔT_t, so any deviation on $\Delta T_{e-\mathrm{wind}}$ can lead to more serious torsional oscillations rather than ΔT_t.

(iv) For the regions (2) and (4) in Figure 3, the value of $(\mathrm{d}f/\mathrm{d}\omega_g)$ is low. So, the damping torque based on $\Delta T_{e-\mathrm{wind}}$ is weak. The torsional modes can appear and affect the stability of the electromechanical system. Designing a wind power stabilizer (WPS) for solving this challenge is proposed.

(v) The VSC HVDC transmission system can manage the power flow using the power electronic converters. Equations (1)–(7) show that $\Delta m_r, \Delta\theta_r$ (the control inputs of rectifier) can affect the electrical torques of the both classical power plant (CPP) and wind power plant. So, it is proposed to design a VSC HVDC-based SDC for improving the stability of the whole power system.

The proposed damping controller for WPP is shown in Figure 5. The damping controller obtains a supplementary damping torque that is in the same phase with the electrical torque. The SDC in Figure 5 is designed with another damping controller for the VSC HVDC, which is discussed below.

The main purpose of designing the SDC based on VSC HVDC, in a hybrid system, is the dynamic stability enhancement of the whole power system. As it is known, in a multimachine system, the excitation of interarea oscillating modes can be another factor in degrading the dynamic stability of the power system. Therefore, it is necessary to ensure that these oscillations are eliminated throughout the

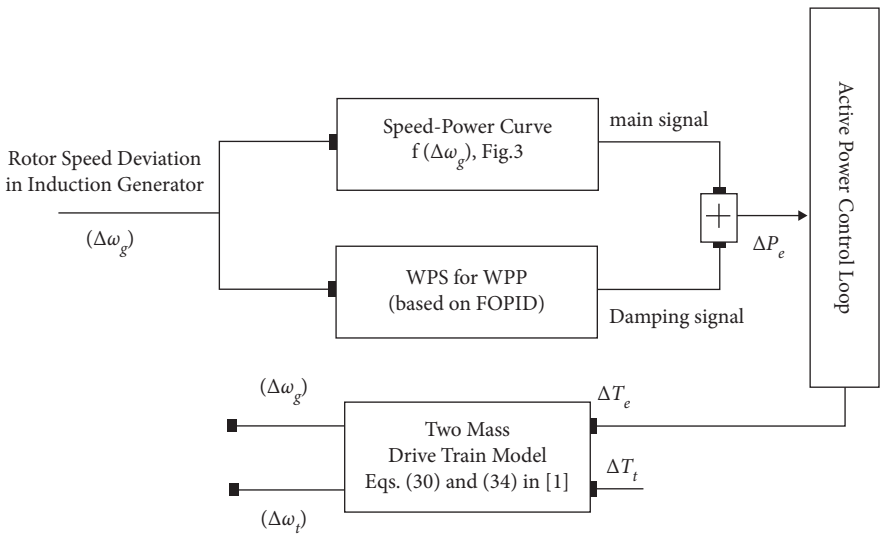

Figure 5: The proposed WPS for the drive train of the WPP.

system especially when a fault accrues. The VSC HVDC-based SDC should be in coordination with wind turbine stabilizer.

Based on equations (1)–(8), rectifier input signals in the VSC HVDC transmission system can affect the electrical power (torque), which is produced by the synchronous or induction generator (η, η' are constant in a determined working point):

$$\Delta T_e \propto \Delta P_e \propto (\eta\theta_r + \eta' m_r). \tag{16}$$

In the VSC HVDC transmission line, it is possible to control the active power flow to prevent frequency deviation (rotor speed deviation in power plants) in the system. Accordingly, the VSC HVDC control inputs can be used to apply a supplementary damping signal [15]. In the next section, the design of the SDC based on the VSC HVDC for the entire power system is described.

4. The VSC HVDC-Based SDC Controller

The relationships between the control inputs of the VSC HVDC and the electrical torques were described in the previous section. Using the rectifier inputs, it is possible to control the power flow between the power plants and infinite bus. Accordingly, the rotor speed deviation in generators can be controlled by changing the input variables of the VSC HVDC using the supplementary controller. For the torsional vibration in the wind turbine, we can write

$$\begin{aligned} \Delta\ddot{\theta}_{tg} + A'\Delta\dot{\theta}_{tg} + B'\Delta\theta_{tg} &= \frac{\Delta T_t}{2H_t} + \frac{\Delta T_{e-\text{wind}}}{2H_g}, \\ \Delta\dddot{\theta}_{tg} + A'\Delta\ddot{\theta}_{tg} + B'\Delta\dot{\theta}_{tg} &= \frac{\Delta\dot{T}_t}{2H_t} + \frac{\Delta\dot{T}_{e-\text{wind}}}{2H_g}. \end{aligned} \tag{17}$$

It can be concluded from the relation (33) that

$$\Delta T_{e-\text{wind}} = f\left(\Delta E'_q, \Delta m_r, \Delta\theta_r, \Delta\omega, \Delta E'_{wd}, \Delta E'_{wq}\right). \tag{18}$$

$\Delta E'_q, \Delta\omega, \Delta E'_{wd}, \Delta E'_{wq}$ are the controllable states of the system and $\Delta m_r, \Delta\theta_r$ are the inputs of the rectifier in the VSC HVDC. Assuming the state variables are constant (and controllable via the typical local control loop such as automatic voltage regulator, etc.), using (1)–(8) and (18), we can write

$$\begin{aligned} \Delta\dot{T}_{e-\text{wind}} &= \alpha\Delta\theta_r + \alpha'\Delta\dot{\theta}_r + \beta\Delta m_r + \beta'\Delta\dot{m}_r \\ &\quad + g\left(\Delta E'_q, \Delta\omega, \Delta E'_{wd}, \Delta E'_{wq}\right), \end{aligned} \tag{19}$$

where g is a function of the system states. Using (19) in equation (17) results in

$$\begin{aligned} \Delta\dddot{\theta}_{tg} + A'\Delta\ddot{\theta}_{tg} + B\prime\Delta\dot{\theta}_{tg} &= \frac{\Delta\dot{T}_t}{2H_t} + \alpha\Delta\theta_r + \alpha'\Delta\dot{\theta}_r + \beta\Delta m_r \\ &\quad + \beta'\Delta\dot{m}_r + g\left(\Delta E'_q, \Delta\omega, \Delta E'_{wd}, \Delta E'_{wq}\right). \end{aligned} \tag{20}$$

Through formula (49), the transfer function with $\Delta m_r, \Delta\theta_r$ as input variables can be derived as follows:

$$\begin{aligned} \frac{\Delta\theta_{tg}}{\Delta m_r} &= \frac{\beta + \beta' s}{S^3 + A's^2 + B's}, \\ \frac{\Delta\theta_{tg}}{\Delta\theta_r} &= \frac{\alpha + \alpha' s}{S^3 + A's^2 + B's}. \end{aligned} \tag{21}$$

The Bode diagram is shown in Figure 4. It can be seen that the rectifier inputs of the VSC HVDC transmission system are quite effective on the torsional modes of the wind turbine system. By designing the SDC, the torsional modes can be damped effectively through these inputs.

It has been shown in many literatures that it is possible to improve the dynamic stability of the power system by using the power electronic converters of the VSC HVDC transmission system. According to [15, 18], it is shown that electromechanical modes are damped optimally using a supplementary damping controller along with the phase

angle input of the rectifier. So, in the hybrid system, it is proposed to use Δm_r for improving the power system oscillations and $\Delta\theta_r$ for damping the torsional vibration of the WPP as it is shown in Figure 6. Notice that the WTS is used to ensure the dynamic stability of the wind turbine (Figure 5).

5. The Supplementary Damping Controller Based on Fractional-Order PID Controller

In this paper, the SDCs are designed for damping the electromechanical oscillations in the hybrid power systems. The proposed controllers can enhance the power system stability. In this way, indicators like the overshoot, settling time, rising time, and steady-state error of the shaft-turbine speed deviation in synchronous generator and induction machine should be optimized.

In this paper, integral absolute error (IAE) is used to define optimization function (x_i is the ith variable):

$$F\left(x_i, i = 1, 2, \ldots, n\right) = \int_0^\infty \left|y(t)^* - y(t)\right| \mathrm{d}t. \tag{22}$$

In equation (51), $y(t)^*$ is the reference and $y(t)$ is the real output response of dynamic system. In this paper, it is proposed to use three ($j = 3$) FOPID-based SDCs in different control loops of system:

(1) The first ($j = 1$) SDC (WTS) is used to obtain supplementary damping torque for ΔP_e as shown in Figure 5. The WTS tries to damp torsional vibrations of WPPs. $\Delta\theta_{tg}$ is the input of WTS.

(2) The second ($j = 2$) and third ($j = 3$) SDCs are used to add supplementary damping signals with different purposes:

(i) The CPP-based SDC signal, which is applied to Δm_r, uses $\Delta\omega$ (rotor speed deviation of synchronous generator in CPP) as input signal. This controller ensures the dynamic stability of the CPP (synchronous generators) in the hybrid power system.

(ii) The WPP-based SDC signal, which is applied to $\Delta\theta_r$, uses $\Delta\theta_{tg}$ (the angular displacement) as input signal. This controller ensures the damping of the torsional vibrations of the wind turbines in the hybrid power system.

The transfer function for the FO-PID controller is shown as follows [24]:

$$G_c(s) = K_p + K_I s^{-\lambda} + K_D s^{\mu}. \tag{23}$$

The IAE for the SDCs design is defined as follows:

$$J\left(K_{pj}, K_{Ij}, K_{Dj}, \lambda_j, \mu_j, j = 1, 2, 3\right) = \int_0^\infty \left(\left|V' - V_{\mathrm{ref}}\right| + \left|\Delta\omega_g\right| + \left|\Delta\omega\right| + \left|\Delta\theta_{tg}\right|\right)\mathrm{d}t. \tag{24}$$

The terminal voltage term ($V' - V_{\mathrm{ref}}$) is used to ensure voltage regulation in the common bus of power plants. The coefficients of FO-PID controller are tuned using the proposed MOBGA. The FO-PID controller includes parameters (which are tuned using EMA) like proportional gain K_p, integral gain K_I, the differential gain K_D, integral-order λ, and differential-order μ.

6. The Multiobjective Bat-Genetic Algorithm

One of the important features of evolutionary algorithms is that they use probability-based solutions to search for the desired space optimally. In this case, two points should be considered [30, 31]:

(i) If a large random space is selected, then the search for all this space will be time consuming; in other words, the convergence to optimal responses will be longer

(ii) In the wide search space, the probability of achieving the optimal responses increases; however, these responses may not be the optimal solutions; in other words, the algorithm may be trapped in local extreme points.

Therefore, it is necessary to always make a compromise between the wide search space and the speed of convergence to the absolute extremum points.

The BA algorithm is based on the bat tracking system [31]. This algorithm uses the frequency adjustment to expand the search space. One of the significant benefits of the BA algorithm is that it focuses on a solution in the search space. This is possible through the delivery rate of the pulses and their frequencies.

This feature of the BA algorithm makes the algorithm highly convergent. At the same time, the chances of getting trapped in local extreme hotspots increase. Therefore, it is necessary to solve this shortcoming of the bat algorithm. In this paper, it is proposed to use genetic algorithm (GA) [30] operators (the mutation and crossover) to diversify the search space as follows:

(1) The particles are arranged based on the particle's cost functions.

(2) The crossover operation in the genetic algorithm are applied for two bats (one has a best cost function and the other is randomly selected from the initial particles) as follows:

$$\begin{aligned} \alpha x_k^1 + (1-\alpha)x_k^2 &= y_k^2, \\ \alpha x_k^2 + (1-\alpha)x_k^1 &= y_k^1, \end{aligned} \tag{25}$$

where (x_k^1, x_k^2) refer to the parent's generation and (y_k^1, y_k^2) refer to the offspring's generation. j is the chromosome of ith step, and k is the multiplier.

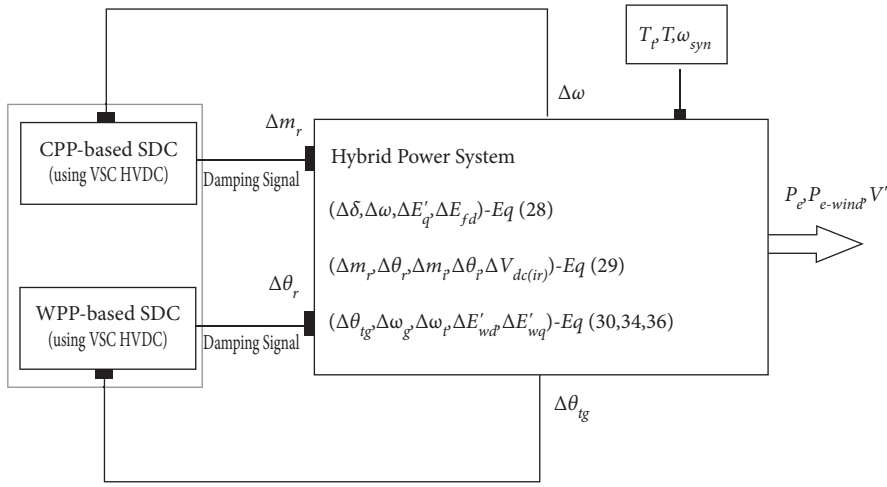

Figure 6: The proposed VSC HVDC-based SDC.

Equation (54) shows the combination of different genes in the GA. This combination will lead to the creation of a new generation using the older ones. Since the old generation was categorized based on its cost function, the new generation (equation (54)) is considered as an upgrade for the older generation.

(3) The resulting generation is modified with some probability to escape from local minima. Dynamic mutations are used in the proposed hybrid genetic-bat algorithm as follows:

$$x_j = \begin{cases} y_j + \left(y^{\max} - y_j\right)(\text{rand})^{(1-\sigma)}, & \text{rand} < 0.5, \\ y_j - \left(y_j - y^{\min}\right)(\text{rand})^{(1-\sigma)}, & \text{rand} > 0.5, \end{cases} \tag{26}$$

where rand, σ, $y^{\max}$, and $y^{\min}$are the random number generator, the constant parameters defined by the user, maximum and minimum values for the variables, respectively. Based on the equation (26), the new generation of bats reproduces with limited oscillations around the old generation. In other words, the range of search space is expanded around the optimal value. If a more appropriate response is obtained, the previous one is replaced. Note that this improvement can prevent the algorithm from the traps of the local extremum points.

If the mutant bat has better performance than the x_j bat, then the particle will move in the same direction; that is, the x_j particle will move to a better location. If the performance of resulting bat is not better than the bat x_j, then it will not move to the new position and the healthier bat will be selected in the next times. The proposed MOBGA is shown in Figure 7.

7. Results and Discussions

In this section, the effect of proposed SDCs on the torsional oscillations of the hybrid power system based on VSC HVDC transmission system (shown in Figure 1) is examined by time domain simulations. All the necessary parameters for the system and proposed MOBGA are given in the appendix. In the simulations, two cases are considered: the case without the SDCs and the case with the proposed damping controllers. Also, the 0.05 pu change of the mechanical power in the CPP is considered as the input disturbance to the system.

The SDCs-based FOPID are designed using the proposed MOBGA. The nominal working condition of the power system is used to design SDCs. In this regard, the cost function defined in equation (53) will be minimized by setting the parameters of the FOPID-based SDCs. Table 1 shows the final coefficients' values of SDCs. The cost function value in each iteration is shown in Figure 8.

Simulation is performed for different scenarios based on the wind speed-power curve of the wind turbine along with the designed SDCs based on FOPID-MOBGA.

In regions (2) and (4) of the speed-power curve (Figure 2), it was shown (refer to Section 3 and Figure 3) that the damping electromechanical torque is not provided for wind turbine effectively. So, it is proposed to add the WTS to the WPP for improving the stability and energy conversion efficiency. Figure 9 shows the responses of system (with SDCs and without SDCs) when the wind turbine works in region 2 ($V_w \approx 8$ m/s). Without the use of SDC, the power system behaves oscillatory. From Figure 9, it can be concluded that using WTS improves the damping of the oscillations by obtaining the supplementary damping electromechanical torque. In this way, the oscillations of the rotor speed deviation in both power plants (Figures 9(a) and 9(b)), angular displacement of rotor in WPP (Figure 9(c)), the load angle deviation in CPP (Figure 9(d)), and the amplitude of the common terminal voltage (Figure 9(e)) are damped with the appropriate value of overshoot and settling time. It has also been observed that by using the proposed SDCs for the VSC HVDC transmission system, further improvement in the damping oscillations of power system components has been achieved.

$\Delta\theta_{tg}$ is shown in Figure 9(c). Without the use of a WTS in the wind turbine and due to the lack of the sufficient damping torque in region (2) of the speed-power curve, the

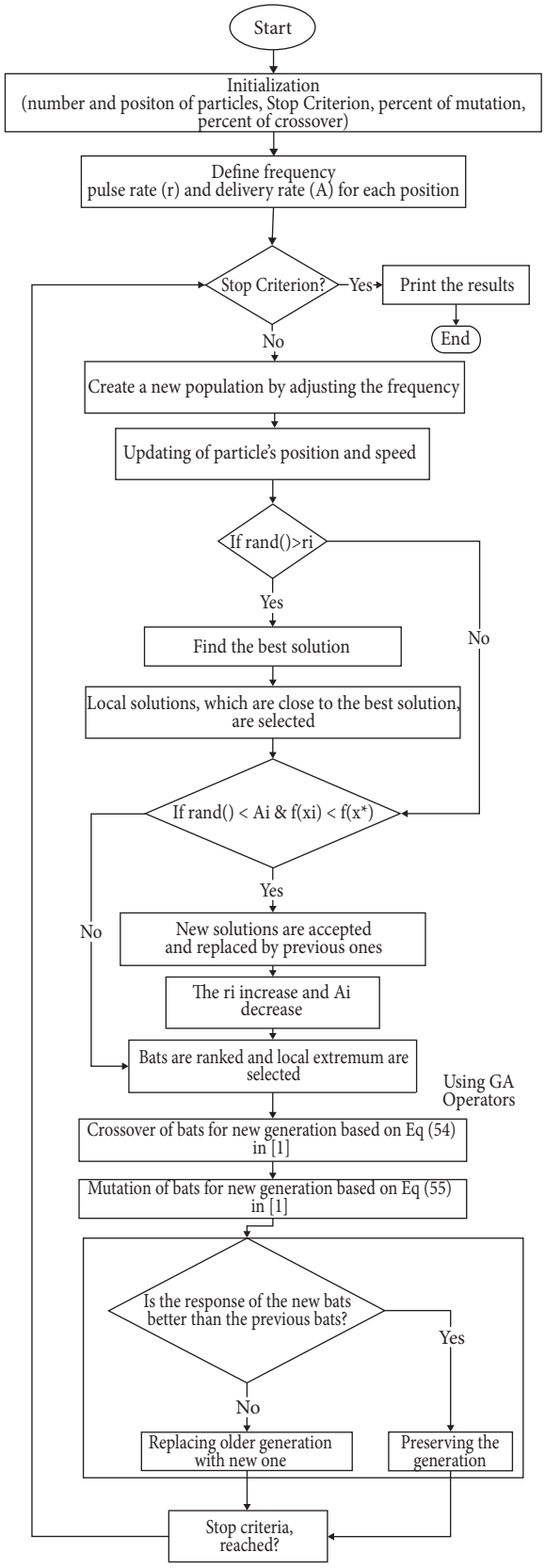

Figure 7: The proposed MOBGA for FOPID designing.

torsional modes in wind turbine have been excited and lead to the oscillations in $\Delta\theta_{tg}$. However, the use of stabilizer in wind turbines has decreased the oscillations. Also, more damping effect of the torsional modes' oscillations is achieved by the SDCs of VSC HVDC. This can increase the quality of energy conversion efficiency in the wind turbine.

V' (the magnitude voltage of the common bus) is shown in Figure 9(e). Using the proposed algorithm, the SDC's coefficients are adjusted in such a way that the minimum terminal voltage deviation is provided. It is observed that the WTS and SDCs have a positive effect on the voltage stabilization.

In region 3 (and 1) of the speed-power curve, the sensitivity of the power-speed curve function to the generator speed is relatively high. So, the generator active power control can provide damping action on the generator speed. Figure 10 shows the responses of system (with SDCs and without SDCs) when the wind turbine works in region 3 ($V_w \approx 12$ m/s). It can be seen that even when the WTS and SDCs are not used, the damping electromagnetic torque is provided by the generator of wind turbine and the system stays stable. Therefore, in this working region, the amplitude of mechanical oscillations is less than 2.

In region 4 of the speed-power curve, the sensitivity of the power-speed curve function to the generator speed is zero. So, the sufficient electromagnetic torque is not obtained by the active power control loop of WPP. Figure 11 shows the responses of system (with SDCs and without SDCs) when the wind turbine works in region 4 ($V_w \approx 14$ m/s). It can be seen that if the WTS or SDCs are not used, the damping electromagnetic torque is not provided by the generator of wind turbine and the system becomes unstable.

The results of the simulation shown in Figures 9–11 are consistent with the analysis presented in Section 3 (depending on the speed-power working regions, the participation of wind turbines in providing the damping torque will be different). If the oscillations of the torsional modes rise in the system, not only the energy conversion efficiency in the wind turbine will be drastically reduced but also more mechanical pressure is imposed on the rotor of the wind turbine. Part (c) of Figures 9–11 shows that the torsional modes of the wind turbine are also affected by the performance of the proposed controllers. It is clear that the oscillations caused by the excitation of the torsional modes are well damped by the proposed controllers.

Part (e) of Figures 9–11 shows that the use of the proposed controllers (SDCs and WTS) not only improves the stability of power system but also can be effective in regulating the voltage of the common bus.

To evaluate the performance of the proposed controllers, the short-circuit (SC) fault (for 7 at $t = 30$ s) in the infinite bus as well as the wind speed change (WSC) (10 percent change at $t = 5$ s up to $t = 15$ s) is applied to the power system. For the comparative purposes, the system is also simulated in the presence of a typical PID controller. The results are shown in Figure 12. Any change in the wind speed also

Table 1: The final coefficients' values of SDCS.

Coefficients	WTS-based SDC	HVDC-based SDC M_r	VSCHVDC-based SDC θ_r
K_p	10.9	12.10	11.6
K_I	28.7	29.3	30.3
K_D	3.9	4.3	4.1
λ	1.29	1.22	1.45
μ	1.02	0.93	1.1

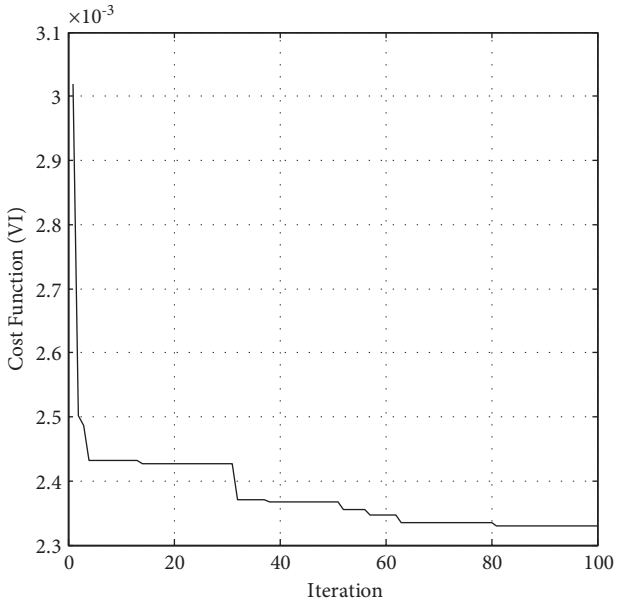

Figure 8: The cost function values in each step.

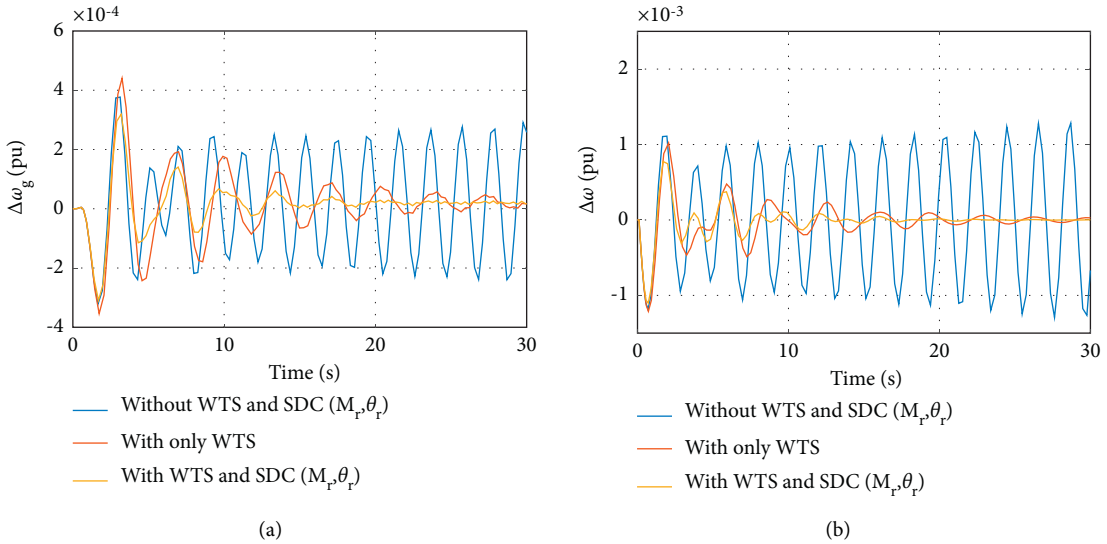

Figure 9: Continued.

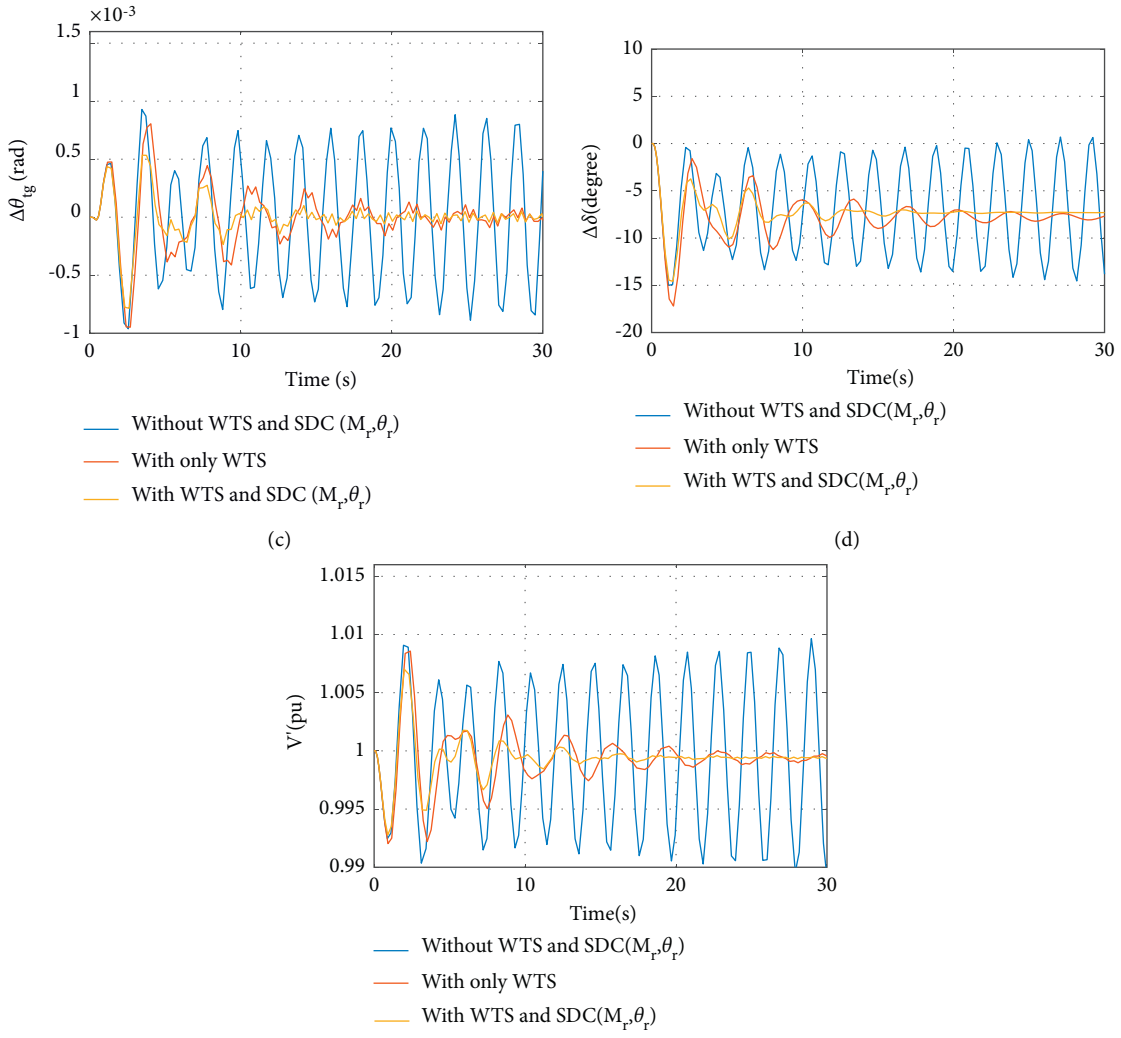

Figure 9: (a) The rotor speed deviation in WPP ($V_w \approx 8$ m/s). (b) The rotor speed deviation in CPP ($V_w \approx 8$ m/s). (c) The angular displacement of rotor in WPP ($V_w \approx 8$ m/s). (d) The load angle deviation in CPP ($V_w \approx 8$ m/s). (e) The common terminal voltage ($V_w \approx 8$ m/s).

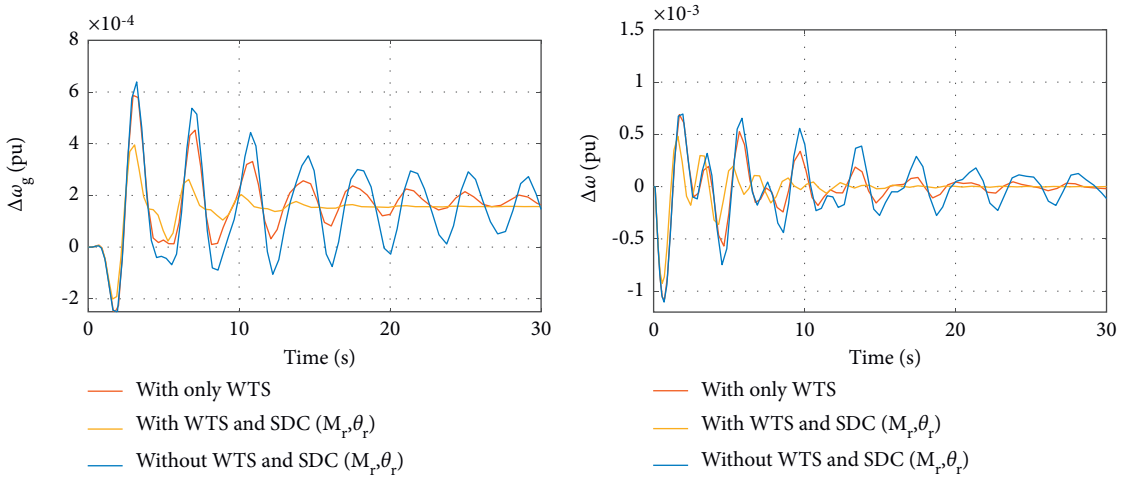

Figure 10: Continued.

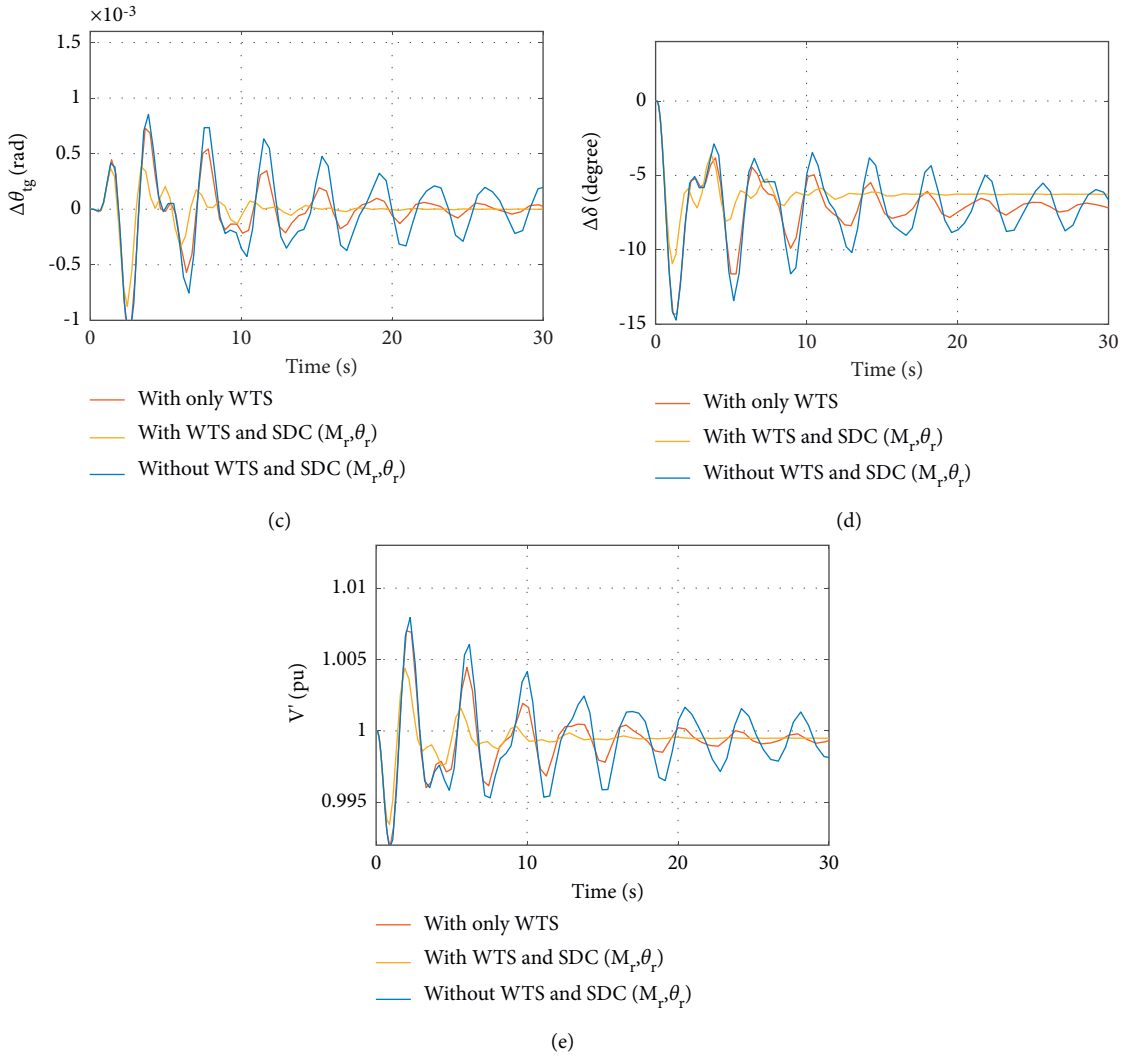

Figure 10: (a) The rotor speed deviation in WPP ($V_w \approx 12$ m/s). (b) The rotor speed deviation in CPP ($V_w \approx 12$ m/s). (c) The angular displacement of rotor in WPP ($V_w \approx 12$ m/s). (d) The load angle deviation in CPP ($V_w \approx 12$ m/s). (e) The common terminal voltage ($V_w \approx 12$ m/s).

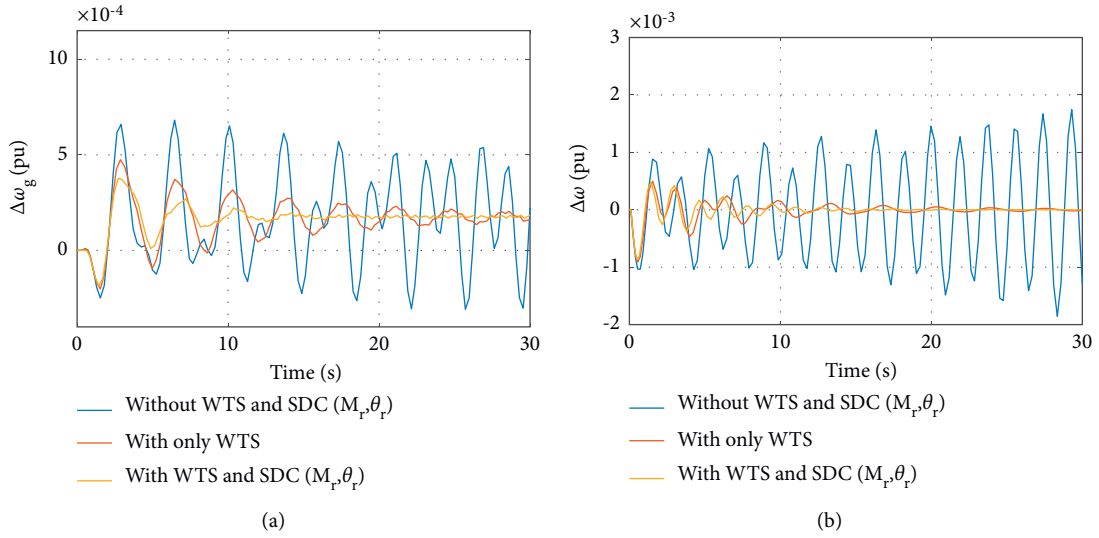

Figure 11: Continued.

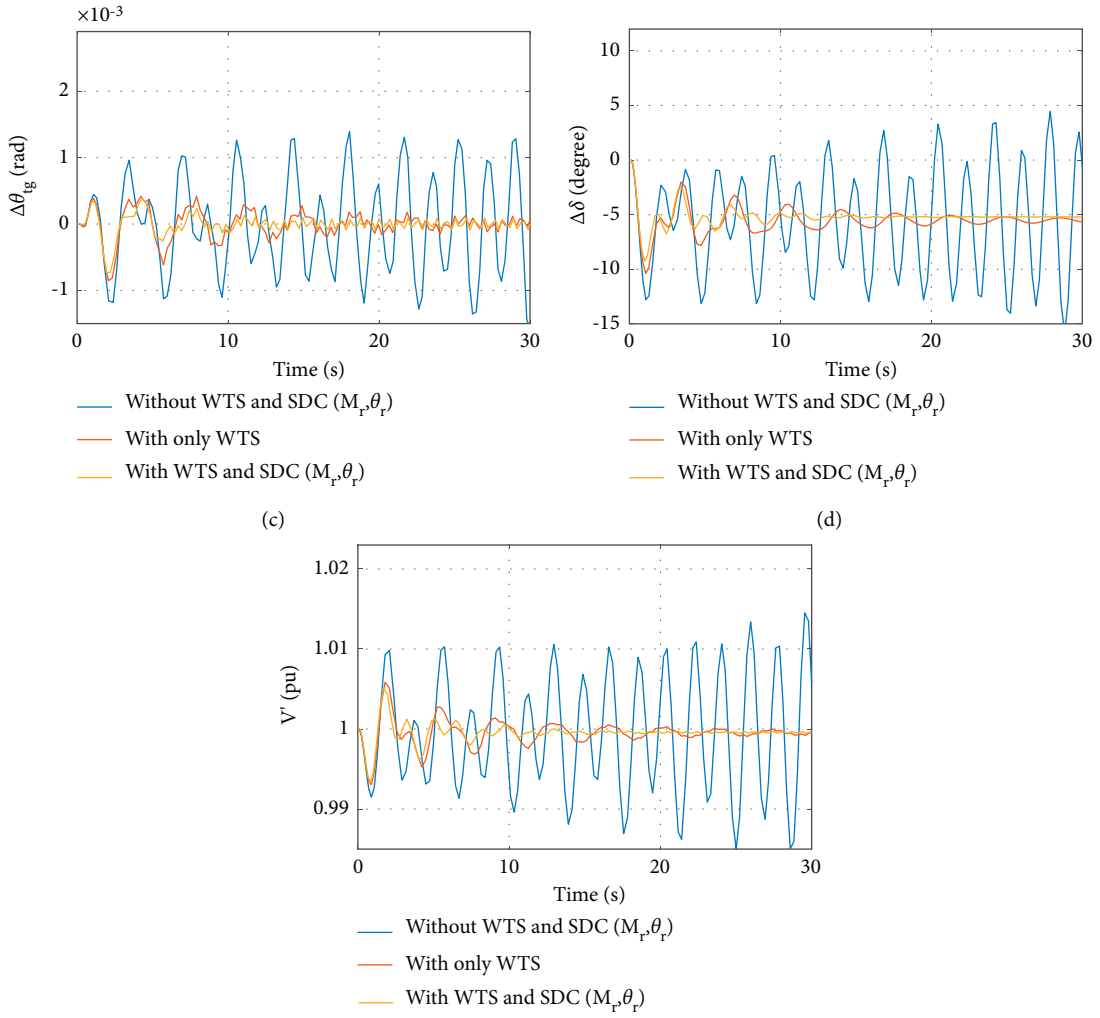

FIGURE 11: (a) The rotor speed deviation in WPP ($V_w \approx 14$ m/s). (b) The rotor speed deviation in CPP ($V_w \approx 14$ m/s). (c) The angular displacement of rotor in WPP ($V_w \approx 14$ m/s). (d) The load angle deviation in CPP ($V_w \approx 14$ m/s). (e) The common terminal voltage ($V_w \approx 14$ m/s).

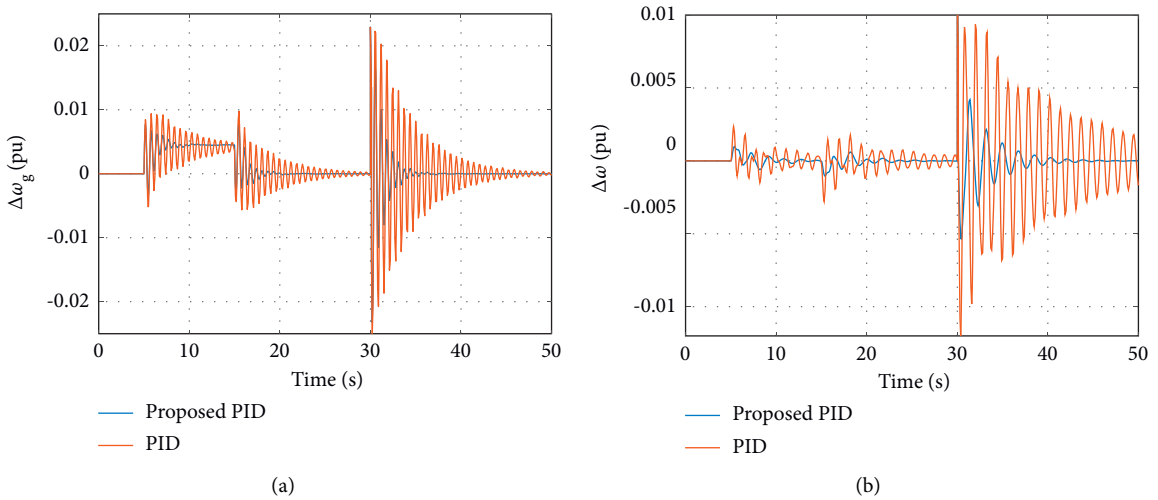

FIGURE 12: Continued.

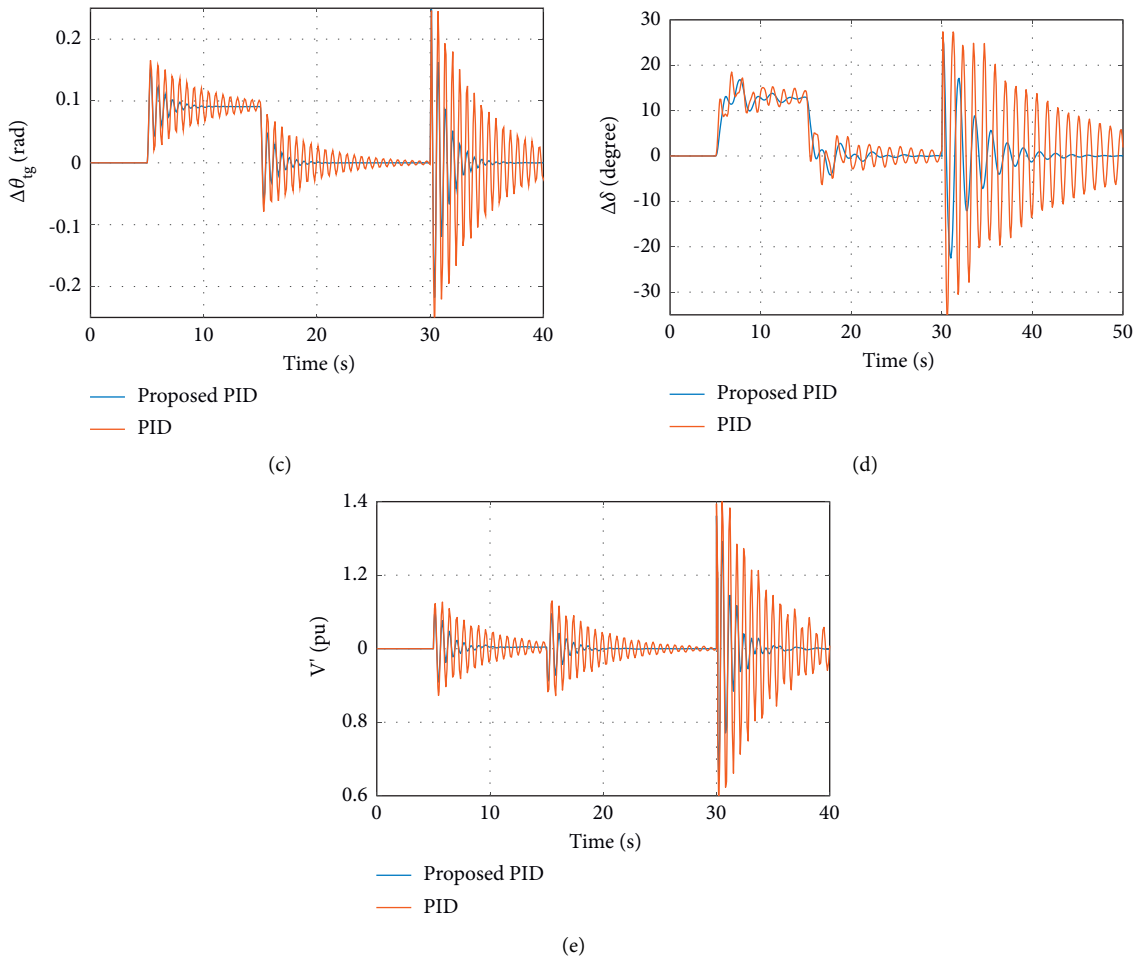

Figure 12: (a) The rotor speed deviation in WPP (SC fault and WSC). (b) The rotor speed deviation in CPP (SC fault and WSC). (c) The angular displacement of rotor in WPP (SC fault and WSC). (d) The load angle deviation in CPP (SC fault and WSC). (e) The common terminal voltage (SC fault and WSC).

changes the working region of the wind turbine. Figures 12(a) and 12(b) show that after the wind speed changes, the power system is still stable and the frequency oscillations are damped. In Figure 12(c), it is observed that the torsional modes are excited when the turbine working speed changes. But using the proposed SDCs, the torsional oscillations are damped effectively. During the short circuit fault in the power system, the oscillation modes of the system are also excited. This causes the frequency-voltage oscillations as shown in Figure 12. The proposed controller not only damps the oscillations of frequency but also improves the voltage profile in the common bus.

8. Conclusions

In this paper, the dynamic model of a power system equipped with a VSC HVDC transmission system and WPP is presented. Using the dynamic equations, the torsional modes of the wind turbine and their impact on the power system stability are evaluated. Dynamic performance of the active control mode of WPP is considered based on the power-speed curve of the wind turbine. It is shown that in regions (2) and (4) of speed-power curve, the electromagnetic damping torque is not sufficient; therefore, the use of the WTS (in these regions) is proposed. Since the control of VSC HVDC transmission systems can be effective in improving the stability of the power system, it is proposed to design SDCs based on the VSC HVDC converters for the hybrid power system. The SDCs and WTS are designed based on FOPID and its coefficients are adjusted using a novel hybrid multiobjective bat-genetic algorithm. The simulation results show that the proposed control strategy of this paper can damp the oscillations caused by the torsional modes of the wind turbine as well as the electromechanical modes of the system.

Data Availability

The data used to support the findings of this study are included in Supplementary Materials files.

Conflicts of Interest

The authors declare that there are no conflicts of interest regarding the publication of this paper.

Supplementary Materials

There are available two files regarding the results of this paper. The first file is a MATLAB m-file named to "Data file.m" as main. The proposed method simulation includes the proposed MOBGA for FOPID designing implementation, which is adjusted using a novel hybrid multiobjective bat-genetic algorithm. This algorithm is also implemented in the m-file, and the result will be shown at the end of simulation. The second file is the data parameters of the power system that is used for simulation in this paper. (*Supplementary Materials*)

References

[1] N. Shafaghtian, A. Kiani, N. Taheri, Z. Rahimkhani, and S. S. Masoumi, "Damping controller design based on FO-PID -EMA in VSC HVDC system to improve stability of hybrid power system," *Journal of Central South University*, vol. 27, no. 2, pp. 403–417, 2020.

[2] G. P. Prajapat, N. Senroy, and I. N. Kar, "Wind turbine structural modeling consideration for dynamic studies of DFIG based system," *IEEE Transactions on Sustainable Energy*, vol. 8, no. 4, pp. 1463–1472, 2017.

[3] M. S. Alam and M. A. Y. Abido, "Fault ride through capability enhancement of a large-scale PMSG wind system with bridge type fault current limiters," *Advances in Electrical and Computer Engineering*, vol. 18, no. 1, pp. 43–50, 2018.

[4] C. P. Ion and I. Serban, "Self-excited induction generator based microgrid with supercapacitor energy storage to support the start-up of dynamic loads," *Advances in Electrical and Computer Engineering*, vol. 18, no. 2, pp. 51–60, 2018.

[5] C. A. Evangelista, A. Pisano, P. Puleston, and E. Usai, "Receding horizon adaptive second-order sliding mode control for doubly-fed induction generator-based wind turbine," *IEEE Transactions on Control Systems Technology*, vol. 25, no. 1, pp. 73–84, 2017.

[6] M. Toulabi, S. Bahrami, and A. M. Ranjbar, "An input-to-state stability approach to inertial frequency response analysis of doubly-fed induction generator-based wind turbines," *IEEE Transactions on Energy Conversion*, vol. 32, no. 4, pp. 1418–1431, 2017.

[7] Y. Zhang, J. Hu, and J. Zhu, "Three-vectors-based predictive direct power control of the doubly fed induction generator for wind energy applications," *IEEE Transactions on Power Electronics*, vol. 29, no. 7, pp. 3485–3500, 2014.

[8] J. J. Justo, F. Mwasilu, and J. W. Jung, "Doubly-fed induction generator-based wind turbines: a comprehensive review of fault ride-through strategies," *Renewable and Sustainable Energy Reviews*, vol. 45, no. 6, 2015.

[9] A. Moharana, R. K. Varma, and R. Seethapathy, "SSR alleviation by STATCOM in induction-generator-based wind farm connected to series compensated line," *IEEE Transactions on Sustainable Energy*, vol. 5, no. 3, pp. 947–957, 2014.

[10] S. Nikkhah and A. Rabiee, "Optimal wind power generation investment, considering voltage stability of power systems," *Renewable Energy*, vol. 115, no. 1, pp. 308–325, 2018.

[11] S. Ma, H. Geng, L. Liu, G. Yang, and B. C. Pal, "Grid-synchronization stability improvement of large-scale wind farm during severe grid fault," *IEEE Transactions on Power Systems*, vol. 33, no. 1, pp. 216–226, 2018.

[12] Y. Xu, M. Yin, Z. Y. Dong, R. Zhang, D. J. Hill, and Y. Zhang, "Robust dispatch of high wind power-penetrated power systems against transient instability," *IEEE Transactions on Power Systems*, vol. 33, no. 1, pp. 174–186, 2018.

[13] A. B. Attya, J. L. Dominguez-Garcia, and O. Anaya-Lara, "A review on frequency support provision by wind power plants: current and future challenges," *Renewable and Sustainable Energy Reviews*, vol. 81, no. 1, pp. 2071–2087, 2018.

[14] Y. Li, L. He, F. Liu et al., "A dynamic coordinated control strategy of WTG-ES combined system for short-term frequency support," *Renewable Energy*, vol. 119, no. 1, pp. 1–11, 2018.

[15] M. R. Banaei and N. Taheri, "An adaptive neural damping controller for HVDC transmission systems," *European Transactions on Electrical Power*, vol. 21, no. 1, pp. 910–923, 2011.

[16] F. H. Gandoman, A. Ahmadi, A. M. Sharaf et al., "Review of FACTS technologies and applications for power quality in smart grids with renewable energy systems," *Renewable and Sustainable Energy Reviews*, vol. 82, no. 1, pp. 502–514, 2018.

[17] A. Hamidi, J. Beiza, E. Babaei, and S. Khanmohammadi, "Adaptive controller design based on input-output signal selection for voltage source converter high voltage direct current systems to improve power system stability," *Journal of Central South University*, vol. 23, no. 9, pp. 2254–2267, 2016.

[18] N. Taheri and M. R. Banaei, "A supplementary neural controller for novel modeling of VSC HVDC to enhance dynamic stability in a power system," in *Proceedings of the 2010 1st Power Electronic & Drive Systems & Technologies Conference (PEDSTC)*, pp. 7–12, IEEE, Tehran, Iran, February 2010.

[19] Y. Guo, H. Gao, Q. Wu, H. Zhao, J. Ostergaard, and M. Shahidehpour, "Enhanced voltage control of VSC-HVDC -connected offshore wind farms based on model predictive control," *IEEE Transactions on Sustainable Energy*, vol. 9, no. 1, pp. 474–487, 2018.

[20] C. Guo, W. Liu, C. Zhao, and X. Ni, "Small-signal dynamics and control parameters optimization of hybrid multi-infeed HVDC system," *International Journal of Electrical Power & Energy Systems*, vol. 98, no. 1, pp. 409–418, 2018.

[21] S. Kundur, Dr. Prabha, J. B. Neal, and G. L. Mark, *Power System Stability and Control*, McGraw-Hill, New York, NY, USA, 1994.

[22] Y. Shen, W. Yao, J. Wen, H. He, and W. Chen, "Adaptive supplementary damping control of VSC-HVDC for interarea oscillation using GrHDP," *IEEE Transactions on Power Systems*, vol. 33, no. 2, pp. 1777–1789, 2018.

[23] Y. Li, G. Tang, T. An et al., "Power compensation control for interconnection of weak power systems by VSC-HVDC," *IEEE Transactions on Power Delivery*, vol. 32, no. 4, pp. 1964–1974, 2017.

[24] O. Kotb, M. Ghandhari, R. Eriksson, R. Leelaruji, and V. K. Sood, "Stability enhancement of an interconnected AC/DC power system through VSC-MTDC operating point adjustment," *Electric Power Systems Research*, vol. 151, no. 1, pp. 308–318, 2017.

[25] M. R. S. Tirtashi, O. Samuelsson, and J. Svensson, "Impedance matching for VSC-HVDC and energy storage damping controllers," *IEEE Transactions on Power Delivery*, vol. 33, no. 2, pp. 1016-1017, 2018.

[26] M. E. C. Bento, "A hybrid particle swarm optimization algorithm for the wide-area damping control design," *IEEE*

Transactions on Industrial Informatics, vol. 18, no. 1, pp. 592–599, 2022.

[27] T. Surinkaew and I. Ngamroo, "Robust power oscillation damper design for DFIG-based wind turbine based on specified structure mixed H2/H∞ control," *Renewable Energy*, vol. 66, pp. 15–24, 2014.

[28] F. M. Hughes, O. Anaya-Lara, N. Jenkins, and G. Strbac, "A power system stabilizer for DFIG-based wind generation," *IEEE Transactions on Power Systems*, vol. 21, no. 2, pp. 763–772, 2006.

[29] T. Surinkaew and I. Ngamroo, "Coordinated robust control of DFIG wind turbine and PSS for stabilization of power oscillations considering system uncertainties," *IEEE Transactions on Sustainable Energy*, vol. 5, no. 3, pp. 823–833, 2014.

[30] T. George and T. Amudha, "Genetic algorithm based multiobjective optimization framework to solve traveling salesman problem," *Advances in Computing and Intelligent Systems*, pp. 141–151, Springer, Berlin, Germany, 2020.

[31] H. Tang, S. Wei, Y. Hongshan, L. Anping, and X. Min, "A multirobot target searching method based on bat algorithm in unknown environments," *Expert Systems with Applications*, vol. 141, Article ID 112945, 2020.